

Experimental Realization of the Markov Chain Monte Carlo Algorithm on a Quantum Computer

Baptiste Claudon,^{1,2,3} Sergi Ramos-Calderer,⁴ and Jean-Philip Piquemal^{1,3}

¹*Qubit Pharmaceuticals, Advanced Research Department, 75014 Paris, France*

²*Sorbonne Université, LJLL, UMR 7198 CNRS, 75005 Paris, France*

³*Sorbonne Université, LCT, UMR 7616 CNRS, 75005 Paris, France**

⁴*Centre for Quantum Technologies, National University of Singapore, Singapore*

(Dated: March 10, 2026)

Quantum algorithms present a quadratically improved complexity over classical ones for certain sampling tasks. For instance, the Quantum Amplitude Estimation (QAE) algorithm promises to speedup the estimation of the mean of certain functions, given access to the quantum state corresponding to the probability distribution to be sampled from. Classically, samples are often obtained by running steps a Markov Chain. In this work, we experimentally use encodings of Markov chains to prepare quantum states and run a quantum Markov Chain Monte Carlo algorithm (qMCMC) on Quantinuum’s H2 and Helios quantum computers. We demonstrate that it is possible to obtain accurate results on current Noisy Intermediate Scale Quantum (NISQ) hardware, operating directly on the physical qubits.

The pursuit of error corrected protocols has seen steady improvement on the quantum hardware. Contemporary quantum devices offer error rates at the point where complex subroutines are starting to be deployed with satisfactory results. While large scale error correction is distant, this early stage offers the opportunity to gauge the development of this technology by pushing the limits of the available hardware. Still, this necessitates a two-pronged approach to be successful. Intimate knowledge of both quantum device and middleware stack is essential to reach optimal performance of the quantum device. Moreover, breakthroughs at the algorithmic level reveal efficient protocols and decompositions that tighten the resources required from the machines in the first place. In this letter we focus on this interplay. We perform a thorough test of the required subroutines for the quantum Markov Chain Monte Carlo algorithm (qMCMC). Diverse encoding techniques are deployed and combined as per the recently proposed quantum encoding of the Metropolis Hastings algorithm [1] on ion trap quantum devices.

Building on Grover’s work [2], Brassard introduced the Quantum Amplitude Estimation algorithm [3]. Given access to quantum states encoding probability distributions, and a reversible algorithm to compute a function, the algorithm yields an estimate of its mean using quadratically fewer resources than the classical Monte Carlo method. Classically, samples from the distribution are often provided by implementing steps of a Markov Chain until the state’s distribution is close enough to its stationary measure. By analogy, it is possible to encode Markov Chains in unitary operations. Such encoding can be used to prepare the quantum state corresponding to the target stationary distribution, and therefore

be used in Brassard’s Quantum Amplitude Estimation (QAE) method.

In this work, we test several encodings of Markov chains on Quantinuum’s H2-1, H2-2 and Helios quantum computers [4–6], focusing on two-state chains. First, we implement a Markov chain using the Linear Combination of Unitaries technique. The resulting encoding is used to sample from the stationary measure, and to estimate an expectation value using the quantum Metropolis–Hastings Markov Chain Monte Carlo (qMCMC) algorithm. Then, we use an encoding method proposed by Szegedy [7] to sample from the stationary distribution. Finally, we test two encoding methods that generalize well in the particular case of Metropolis-Hastings walks [1, 8]. The first is a modification of Szegedy’s method, the second is closer to Szegedy’s quantization method and encodes a process on the pairs of states. We use the first method to sample from the stationary distribution and verify that the corresponding quantum state is indeed an eigenvector of the second encoding method.

I. QUANTUM MARKOV CHAIN MONTE CARLO

Let \mathbb{S} be a finite state space of size n . A Markov kernel is a matrix P of positive numbers and size $n \times n$ such that $\sum_{y \in \mathbb{S}} P(x, y) = 1$, for all $x \in \mathbb{S}$. Throughout this work, we restrict to ergodic Markov chains, admitting a unique stationary distribution π satisfying $\pi P = \pi$ and $\pi(x) > 0$ for all $x \in \mathbb{S}$. We denote the coherent encoding of a probability distribution μ by $|\mu\rangle = \sum_{x \in \mathbb{S}} \sqrt{\mu(x)} |x\rangle$. In particular, $|\pi\rangle$ denotes the stationary state. Ref. [9] provides a detailed exposition of the properties of such ergodic Markov kernels.

Quantum algorithms for Markov chains rely on embedding non-unitary stochastic operators into larger unitary operators. We here give a precise definition of such en-

* Contact authors: baptiste.claudon@qubit-pharmaceuticals.com, jean-philip.piquemal@sorbonne-universite.fr

coding [10].

Definition 1 Let U be a unitary acting on a Hilbert space \mathcal{H} , and let $\square : \mathbb{C}^n \rightarrow \mathcal{H}$ be a partial isometry. If U is symmetric, then (U, \square) is called a Symmetric Projected Unitary Encoding of an operator A if $\square^\dagger U \square = A$.

These Symmetric Projected Unitary Encodings (SPUEs) naturally arise in quantum walk constructions. In practice, different implementations of \square and U correspond to different realizations of the same effective operator A . In this work we focus on experimentally comparing several such encodings.

Given a SPUE, one can construct a quantum walk operator whose spectrum is directly related to that of the encoded symmetric operator. This can be stated more precisely as follows.

Definition 2 Let (U, \square) be a SPUE of an operator A . Its associated qubitized walk operator is

$$\mathcal{W} = (2\square\square^\dagger - 1)U. \quad (1)$$

These SPUEs become the basis on which the quantum walk encoding is built from. The following theorem underlies all subsequent algorithms [7, 10].

Theorem 1 Let (U, \square) be a SPUE of an operator A , with qubitized walk operator \mathcal{W} . Let $\lambda \in]-1, 1[$ be an eigenvalue of A with eigenvector $|v\rangle$. Define $\theta = \cos^{-1}(\lambda)$. Then \mathcal{W} has eigenvalues $e^{\pm i\theta}$ with eigenvectors supported on the two-dimensional invariant subspace spanned by $\square|v\rangle$ and $U\square|v\rangle$. If $\lambda = \pm 1$, then $\square|v\rangle$ is an eigenvector of \mathcal{W} with the same eigenvalue.

From here, the qubitized walk operator follows. Given a Markov kernel P , define the quantum step operator

$$\square = \sum_{x \in \mathbb{S}} |x\rangle |P(x, \cdot)\rangle \langle x|. \quad (2)$$

For reversible chains with stationary distribution π , the discriminant matrix

$$\mathcal{D}(x, y) = \sqrt{\frac{\pi(x)}{\pi(y)}} P(x, y) \quad (3)$$

is symmetric and shares the same spectrum as P . Using the SWAP operator S , the pair (S, \square) is a SPUE of \mathcal{D} . This is referred to as Szegedy's quantization method [7]. The associated qubitized walk operator therefore encodes the spectral properties of the original Markov chain. Importantly, the stationary state $|\pi\rangle$ satisfies $\mathcal{D}|\pi\rangle = |\pi\rangle$ and corresponds to the unique 1 eigenstate of the walk operator in the range of \square . However, other partial isometries and unitary operators can also encode the discriminant matrix.

Let \mathcal{W} denote the qubitized walk operator of a reversible ergodic chain. Since $\square|\pi\rangle$ is the unique eigenvector of \mathcal{W} with eigenvalue 1, it can be prepared using

phase estimation [11, 12]. Recall that given an eigenvector $|\psi\rangle$ of \mathcal{W} with eigenvalue $e^{2\pi i\phi}$, $\phi \in \{k/2^t\}_{k=0}^{2^t-1}$, the phase estimation of \mathcal{W} maps $|\psi\rangle|0\rangle$ to $|\psi\rangle|2^t\phi\rangle$. Together with post-selection, the algorithm can also serve to prepare eigenstates.

Ultimately, the target expectation value of the desired observable is extracted via amplitude estimation as follows. Let $f : \mathbb{S} \rightarrow [0, 1]$ be an observable. The Monte Carlo algorithm aims at estimating

$$\mathbb{E}_\pi(f) = \pi f = \sum_{x \in \mathbb{S}} \pi(x) f(x). \quad (4)$$

We assume access to f through a unitary O_f such that

$$O_f |x, 0\rangle = \sqrt{f(x)} |x, 0\rangle + \sqrt{1-f(x)} |x, 1\rangle. \quad (5)$$

Applied to $|\pi, 0\rangle$, O_f yields the state

$$|\pi \cdot f\rangle = \sum_{x \in \mathbb{S}} \sqrt{\pi(x)f(x)} |x, 0\rangle + \sqrt{\pi(x)(1-f(x))} |x, 1\rangle. \quad (6)$$

In particular, $(2|\pi \cdot f\rangle \langle \pi \cdot f| - 1, |0\rangle)$ is a SPUE of the symmetric operator

$$2 \langle 0 | \pi \cdot f \rangle \langle \pi \cdot f | 0 \rangle - 1, \quad (7)$$

with eigenvalues -1 and $2\pi f - 1$. Thus, applying the phase estimation algorithm to the qubitized walk operator of $(2|\pi \cdot f\rangle \langle \pi \cdot f| - 1, |0\rangle)$ and initial state $|\pi \cdot f\rangle$ yields eigenvalue phases $\pm \cos^{-1}(2\pi f - 1)$. Taking the cosine of either measured phase gives $2\pi f - 1$.

II. RESULTS

In our experiments, we consider a two-state-space $\mathbb{S} = \{0, 1\}$ and Markov kernels of the form

$$P = \begin{pmatrix} 1-\delta & \delta \\ \delta & 1-\delta \end{pmatrix}, \delta > 0. \quad (8)$$

Such Markov kernel has uniform stationary measure: $\pi = (0.5 \ 0.5)$. For the first set of experiments, we will consider $\delta = 1/4$.

The presented results are obtained through Quantinuum's *nexus* platform [13], using *pytket* [14] for the H2 deployment and *guppylang* [15] for Helios.

A. State preparation and amplitude estimation

Linear Combination of Unitaries. Notice that P can be written as the weighted sum of two unitary operators, $P = (1-\delta)I + \delta X$, where I is the two-by-two identity matrix and $X = |0\rangle\langle 1| + |1\rangle\langle 0|$. Define the two-qubit unitary U by:

$$a: \begin{array}{c} \text{---} \\ \text{---} \end{array} \begin{array}{c} \boxed{U} \\ \text{---} \\ \text{---} \end{array} \begin{array}{c} \text{---} \\ \text{---} \end{array} = a: \begin{array}{c} \text{---} \\ \text{---} \end{array} \begin{array}{c} \boxed{R_Y(\theta)} \\ \text{---} \\ \text{---} \end{array} \begin{array}{c} \bullet \\ \text{---} \\ \oplus \end{array} \begin{array}{c} \boxed{R_Y(-\theta)} \\ \text{---} \\ \text{---} \end{array} \begin{array}{c} \text{---} \\ \text{---} \end{array}, \quad (9)$$

where $\theta = \cos^{-1}(\sqrt{1-\delta}) = \pi/6$, a labels the ancilla qubit and x the state space qubit. Then, $(U, |0\rangle)$ is a SPUE of P (where $|0\rangle$ is the state of the qubit a). The corresponding qubitized walk operator is $\mathcal{W} = ZU$, where Z acts on the qubit a , and can easily be controlled by a control qubit c , as shown on Figure 1. Note that $(\mathcal{W}^3, |0\rangle)$ is a SPUE of $2|\pi\rangle\langle\pi| - 1$. It can be used as in Figure 2 to prepare $|\pi\rangle$. Moreover, the compiled circuit can be found in Appendix A, Figure 5.

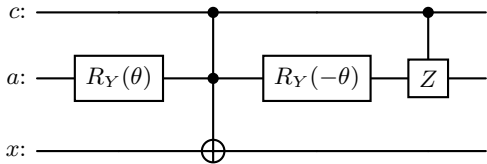


FIG. 1. Controlled- \mathcal{W} circuit. c labels the control qubit, a the ancilla qubit and x the state space qubit.

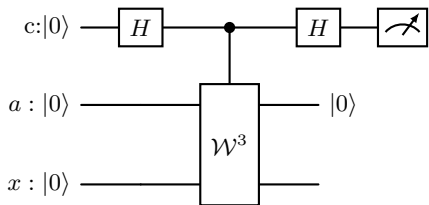


FIG. 2. State preparation circuit. c labels the control qubit, a the ancilla qubit and x the state space qubit. If the control qubit is measured in state $|0\rangle$, the ancilla qubit exits in state $|0\rangle$ and the state qubit in state $|\pi\rangle$.

Table I gathers the sampling statistics obtained from measuring the state preparation circuit.

	$x: 0\rangle$	$x: 1\rangle$	Number of successes $ \{c=0\} $
H2-1	2586	2447	5033
Helios	2321	2459	4780
Expected	2500	2500	5000

TABLE I. State preparation measurements with initial state $|0\rangle$ and 10^4 shots using linear combination of unitaries.

Table II gathers the amplitude estimation statistics, when computing the mean of the function $f(x) = \delta_1(x)$, such that $\mathbb{E}_\pi(f) = 1/2$. The compiled circuit can be found in Appendix A, Figure 6.

Szegedy Walk. Alternatively, P can be encoded following Szegedy's quantization procedure [7]. This method requires a unitary O such that:

$$O|0,0\rangle = \sqrt{1-\delta}|0,0\rangle + \sqrt{\delta}|0,1\rangle, \quad (10)$$

and

$$O|1,0\rangle = \sqrt{\delta}|1,0\rangle + \sqrt{1-\delta}|1,1\rangle. \quad (11)$$

Measured $E_\pi(f)$:	0	0.5	1
H2-1	12	444	29
Helios	8	464	16
Expected	0	500	0

TABLE II. Measurements of $E_\pi(f)$ with 10^3 shots via the linear combination of unitaries method. The state preparation was successful 485 times on H2-1 and 488 times on Helios.

A possible implementation of O is given in Figure 3. Then, $(S, O|0\rangle, O|0\rangle)$ will be a SPUE of P . The corresponding qubitized walk operator is $\mathcal{W} = OZO^\dagger S$ and can be used as in Figure 2 to prepare $|\pi\rangle$. Table III reports the samples obtained using Szegedy's method. The compiled circuit can be found in Appendix A, Figure 7.

x, y :	$ 00\rangle$	$ 01\rangle$	$ 11\rangle$	$ 10\rangle$
H2-1	1711	694	1779	625
Helios	2054	543	1743	662
Expected	1875	625	1875	625

x :	$ 0\rangle$	$ 1\rangle$
H2-1	2405	2404
Helios	2597	2405
Expected	2500	2500

TABLE III. State preparation using Szegedy's method. The state preparation was successful 4932 times over 10^4 shots, following from the predicted success rate of 0.5.

Controlled-SWAP Encoding. Yet another way to encode P is to see it as a Metropolis-Hastings kernel. The proposal kernel is $T = X$ and each move is accepted with probability δ . In our experiment, we consider $O_A = \exp(i\pi Y/6)$ and

$$O_T = \begin{array}{c} x: \\ y: \end{array} \left[\begin{array}{c} \text{ } \\ \text{ } \\ \text{ } \end{array} \right] = \begin{array}{c} x: \\ y: \end{array} \left[\begin{array}{c} \text{ } \\ \oplus \\ \oplus \end{array} \right]. \quad (13)$$

Then, $(S^c, O_A O_T |0,0\rangle)$ is a SPUE of P . We prepare the state $O_A O_T |\pi, 0, 0\rangle$, measure the x -qubit and the phase qubit. The compiled circuit can be found in Appendix A, Figure 8. The measurement statistics are reported in Table IV.

x :	$ 0\rangle$	$ 1\rangle$	Number of phase 0 measurements
H2-1	4948	4732	9680
Helios	5013	4738	9751
Expected	5000	5000	10000

TABLE IV. State preparation using the controlled-SWAP method.

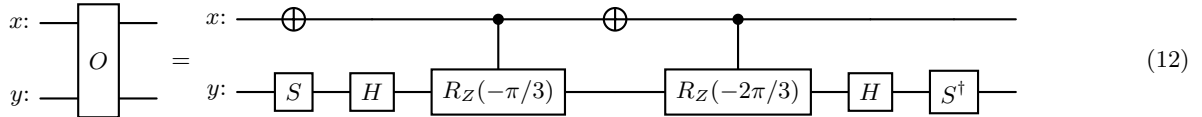


FIG. 3. Quantum circuit implementing the unitary O in Szegedy’s quantization procedure.

B. Dual Space quantum Markov Chain Monte Carlo

For every Metropolis Hastings kernel, using only O_T and O_A , it is possible to encode the quantum step operator of a Markov process on the pairs of possible state and whose first marginal is a Metropolis Hastings Markov chain. Working on this dual space avoids the costly overhead needed to keep track of acceptance/rejection probabilities. The construction of the corresponding qubitized walk operator \mathcal{W} is given in full generality [1] and we give the corresponding circuit for $T = X$ and $O_A = e^{i\pi Y/4}$ in Appendix A, Figure 9. To validate the correct implementation of the qubitized walk operator, we design and deploy the following experiment. The kernel’s one-eigenstate is prepared using a unitary V on the initial state $|0\rangle$. We verify its implementation fidelity by measuring its computational basis statistics. The qubitized walk operator is then applied to this state and the same computational basis statistics are measured. We expect the statistics to be the same. Figure 4 illustrates the results obtained on the H2-1, H2-2 and Helios devices. In addition to the raw measurement statistics, we estimate the overlap $|\langle 0|V^\dagger\mathcal{W}V|0\rangle|^2$ by measuring $V^\dagger\mathcal{W}V|0\rangle$. The number of measured 0 is reported in Table V. The eigenstate corresponds to the SPUE ancilla in state $|+\rangle$, the intail-inhead qubits in state $\frac{1}{\sqrt{2}}(|01\rangle + |10\rangle)$, the outtail-outhead qubits in state $\frac{1}{\sqrt{2}}(|01\rangle + |10\rangle)$. All other qubits are expected in state $|0\rangle$. Writing the computational basis states in base 10, the eigenstate is:

$$V|0\rangle = \frac{1}{\sqrt{8}} (|10\rangle + |12\rangle + |18\rangle + |20\rangle + |42\rangle + |44\rangle + |50\rangle + |52\rangle). \quad (14)$$

Device	H2-1	H2-2	Helios	Expected
$ 0\rangle$ measurements	688	650	707	1000

TABLE V. Number of 0 outcomes when measuring $V^\dagger\mathcal{W}V|0\rangle$, over 1000 shots.

III. DISCUSSION

In this work, we deploy on two ion trap quantum devices several projected unitary encodings of Markov ker-

nels and their qubitized walk operators. The results provide a good picture of the present state-of-the-art realizations of quantum Markov Chain Monte Carlo algorithms.

First, we used a phase estimation algorithm to prepare the stationary measure of a Markov chain encoded with a Linear Combination of Unitaries technique. With successful results. The prepared state is then used to estimate the mean of a simple function using the Quantum Amplitude Estimation algorithm. The algorithm consists of 237 gates acting on 6 qubits. It yields the right expectation value estimate in 90% of the experiments. We then repeated the stationary state preparation using Szegedy’s method. Once again, the experimental results are in perfect agreement with the theory: the success rate is of 0.5, as determined by the squared overlap between the starting distribution and the stationary measure. Then, we applied a phase estimation algorithm of the qubitized walk operator to the expected stationary state of the controlled-SWAP method. The expected 0 phase was measured with a success rate of 93%. Finally, we tested the qubitized walk operator associated with the dual Metropolis Hastings kernels. We measured the squared overlap between the 1 eigenvector before and after applying the qubitized walk operator to be about 2/3, with the Helios machine yielding best results. This shows that circuits sizes of 500 appear to be the current limits of the H2 and Helios Noisy Intermediate Scale Quantum (NISQ) devices.

Our results show that, at the current noise levels, circuits of depth corresponding to roughly 250 elementary gates can still yield quantitatively meaningful Monte Carlo estimates, even when applied directly to the physical qubits. A natural next step is to perform analogous experiments or experiments targeting nonreversible Markov chains [16] on next-generation devices. Their improved gate quality may lead to more accurate results and allow for larger experiments. It would also be valuable to run error corrected versions of these quantum circuits. Hopefully, we would observe lower error rates on the logical qubits compared to the present physical qubits. Ultimately, these implementations provide a decisive proof of concept for scaling quantum hardware simulations. By leveraging the full quadratic speedups of Markov Chain Monte Carlo algorithms, this approach offers broad utility across statistical physics, computational chemistry, Bayesian inference, and machine learning optimization.

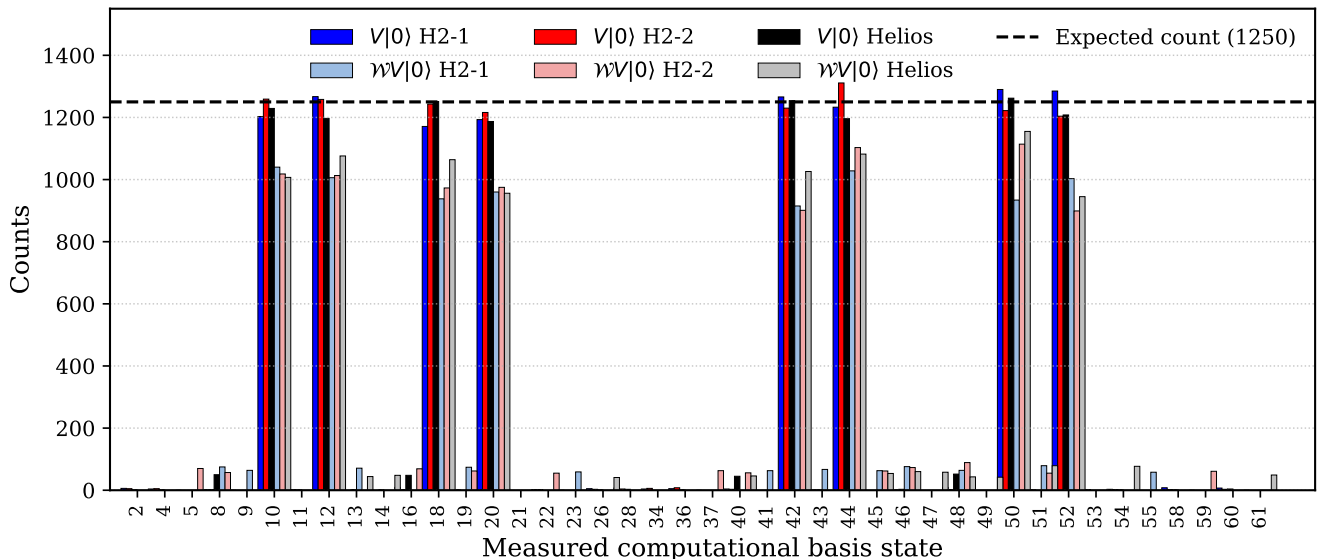


FIG. 4. Measurement statistics of 10^4 measurements of $V|0\rangle$ and $\mathcal{W}V|0\rangle$ on Quantinuum’s H2-1, H2-2 and Helios devices. We expect $V|0\rangle$ to be a 1 eigenvector of \mathcal{W} , thus should remain unchanged after the application of the walk operator. The eigenstate is $V|0\rangle = \mathcal{W}V|0\rangle = \frac{1}{\sqrt{8}}(|10\rangle + |12\rangle + |18\rangle + |20\rangle + |42\rangle + |44\rangle + |50\rangle + |52\rangle)$.

IV. ACKNOWLEDGMENTS

This work has received funding from the European Research Council (ERC) under the European Union’s Horizon 2020 research and innovation program (grant agreement No 810367), project EMC2 (JPP). Computations on the H2 machines have been made possible through the Quantinuum Startup Partner Program. The authors

thank the National Quantum Office, Singapore, for providing computing time on the Quantinuum Helios system.

V. REFERENCES

-
- [1] B. Claudon, P. Rodenas-Ruiz, J.-P. Piquemal, and P. Monmarché, Quantum circuits for the metropolis-hastings algorithm (2025), arXiv:2506.11576 [quant-ph].
- [2] L. K. Grover, A fast quantum mechanical algorithm for database search, in *Proceedings of the Twenty-Eighth Annual ACM Symposium on Theory of Computing*, STOC ’96 (Association for Computing Machinery, New York, NY, USA, 1996) p. 212–219.
- [3] G. Brassard, P. Høyer, M. Mosca, and A. Tapp, Quantum amplitude amplification and estimation (2002).
- [4] J. M. Pino, J. M. Dreiling, C. Figgatt, J. P. Gaebler, S. A. Moses, M. S. Allman, C. H. Baldwin, M. Foss-Feig, D. Hayes, K. Mayer, C. Ryan-Anderson, and B. Neyenhuis, Demonstration of the trapped-ion quantum ccd computer architecture, *Nature* **592**, 209–213 (2021).
- [5] S. A. Moses, C. H. Baldwin, M. S. Allman, R. Ancona, L. Ascarrunz, C. Barnes, J. Bartolotta, B. Bjork, P. Blanchard, M. Bohn, J. G. Bohnet, N. C. Brown, N. Q. Burdick, W. C. Burton, S. L. Campbell, J. P. Campora, C. Carron, J. Chambers, J. W. Chan, Y. H. Chen, A. Chernoguzov, E. Chertkov, J. Colina, J. P. Curtis, R. Daniel, M. DeCross, D. Deen, C. Delaney, J. M. Dreiling, C. T. Ertsgaard, J. Esposito, B. Estey, M. Fabrikant, C. Figgatt, C. Foltz, M. Foss-Feig, D. Francois, J. P. Gaebler, T. M. Gatterman, C. N. Gilbreth, J. Giles, E. Glynn, A. Hall, A. M. Hankin, A. Hansen, D. Hayes, B. Higashi, I. M. Hoffman, B. Horning, J. J. Hout, R. Jacobs, J. Johansen, L. Jones, J. Karcz, T. Klein, P. Lauria, P. Lee, D. Liefer, S. T. Lu, D. Lucchetti, C. Lytle, A. Malm, M. Matheny, B. Mathewson, K. Mayer, D. B. Miller, M. Mills, B. Neyenhuis, L. Nugent, S. Olson, J. Parks, G. N. Price, Z. Price, M. Pugh, A. Ransford, A. P. Reed, C. Roman, M. Rowe, C. Ryan-Anderson, S. Sanders, J. Sedlacek, P. Shevchuk, P. Siegfried, T. Skripka, B. Spaun, R. T. Sprenkle, R. P. Stutz, M. Swallows, R. I. Tobey, A. Tran, T. Tran, E. Vogt, C. Volin, J. Walker, A. M. Zolot, and J. M. Pino, A race-track trapped-ion quantum processor, *Phys. Rev. X* **13**, 041052 (2023).
- [6] A. Ransford, M. S. Allman, J. Arkininstall, J. P. C. III, S. F. Cooper, R. D. Delaney, J. M. Dreiling, B. Estey, C. Figgatt, A. Hall, A. A. Husain, A. Isanaka, C. J. Kennedy, N. Kotibhaskar, I. S. Madjarov, K. Mayer, A. R. Milne, A. J. Park, A. P. Reed, R. Ancona, M. P.

- Andersen, P. Andres-Martinez, W. Angenent, L. Argueta, B. Arkin, L. Ascarrunz, W. Baker, C. Barnes, J. Bartolotta, J. Berg, R. Besand, B. Bjork, M. Blain, P. Blanchard, R. Blume-Kohout, M. Bohn, A. Borgna, D. Y. Botamanenko, R. Boutelle, N. Brown, G. T. Buckingham, N. Q. Burdick, W. C. Burton, V. Carey, C. J. Carron, J. Chambers, J. Children, V. E. Colussi, S. Crepinsek, A. Cureton, J. Davies, D. Davis, M. De-Cross, D. Deen, C. Delaney, D. DelVento, B. J. DeSalvo, J. Dominy, R. Duncan, V. Eccles, A. Edgington, N. Erickson, S. Erickson, C. T. Ertsgaard, B. Evans, T. Evans, M. I. Fabrikant, A. Fischer, C. Foltz, M. Foss-Feig, D. Francois, B. Freyberg, C. Gao, R. Garay, J. Garvin, D. M. Gaudiosi, C. N. Gilbreth, J. Giles, E. Glynn, J. Graves, A. Hansen, D. Hayes, L. Heidemann, B. Higashi, T. Hilbun, J. Hines, A. Hlavaty, K. Hoffman, I. M. Hoffman, C. Holliman, I. Hooper, B. Horning, J. Hostetter, D. Hothem, J. Houlton, J. Hout, R. Hutson, R. T. Jacobs, T. Jacobs, M. Johannsen, J. Johansen, L. Jones, S. Julian, R. Jung, A. Keay, T. Klein, M. Koch, R. Kondo, C. Kong, A. Kosto, A. Lawrence, D. Liefer, M. Lollie, D. Lucchetti, N. K. Lysne, C. Lytle, C. MacPherson, A. Malm, S. Mather, B. Mathewson, D. Maxwell, L. McCaffrey, H. McDougall, R. Mendoza, M. Mills, R. Morrison, L. Narmour, N. Nguyen, L. Nugent, S. Olson, D. Ouellette, J. Parks, Z. Peters, J. Petricka, J. M. Pino, F. Polito, M. Preidl, G. Price, T. Proctor, M. Pugh, N. Ratcliff, D. Raymondson, P. Rhodes, C. Roman, C. Roy, C. Ryan-Anderson, F. B. Sanchez, G. Sangiolo, T. Sawadski, A. Schaffer, P. Schow, J. Sedlacek, H. Semenenko, P. Shevchuk, S. Shore, P. Siegfried, K. Singhal, S. Sivarajah, T. Skripka, L. Sletten, B. Spaun, R. T. Sprenkle, P. Stoufer, M. Tader, S. F. Taylor, T. H. Thompson, R. Tobey, A. Tran, T. Tran, G. Vittorini, C. Volin, J. Walker, S. White, D. Wilson, Q. Wolf, C. Wringe, K. Young, J. Zheng, K. Zuraski, C. H. Baldwin, A. Chernoguzov, J. P. Gaebler, S. J. Sanders, B. Neyenhuis, R. Stutz, and J. G. Bohnet, Helios: A 98-qubit trapped-ion quantum computer (2025), arXiv:2511.05465 [quant-ph].
- [7] M. Szegedy, Quantum speed-up of markov chain based algorithms, in *45th Annual IEEE Symposium on Foundations of Computer Science* (2004) pp. 32–41.
- [8] W. K. Hastings, Monte carlo sampling methods using markov chains and their applications, *Biometrika* **57**, 97 (1970), <https://academic.oup.com/biomet/article-pdf/57/1/97/23940249/57-1-97.pdf>.
- [9] D. A. Levin, Y. Peres, and E. L. Wilmer, *Markov chains and mixing times* (American Mathematical Society, 2006).
- [10] C. Sünderhauf, Generalized quantum singular value transformation (2023), arXiv:2312.00723 [quant-ph].
- [11] A. Y. Kitaev, Quantum measurements and the abelian stabilizer problem (1995), arXiv:quant-ph/9511026 [quant-ph].
- [12] M. A. Nielsen and I. L. Chuang, *Quantum Computation and Quantum Information* (Cambridge University Press, 2000).
- [13] Quantinuum nexus (2024).
- [14] S. Sivarajah, S. Dilkes, A. Cowtan, W. Simmons, A. Edgington, and R. Duncan, t—ket): a retargetable compiler for nisq devices, *Quantum Science and Technology* **6**, 014003 (2020).
- [15] M. Koch, A. Lawrence, K. Singhal, S. Sivarajah, and R. Duncan, Guppy: pythonic quantum-classical programming, arXiv preprint arXiv:2510.12582 (2025).
- [16] B. Claudon, J.-P. Piquemal, and P. Monmarché, Quantum speedup for nonreversible markov chains, *Nature Communications* **16**, 10.1038/s41467-025-65761-5 (2025).

Appendix A: Circuits

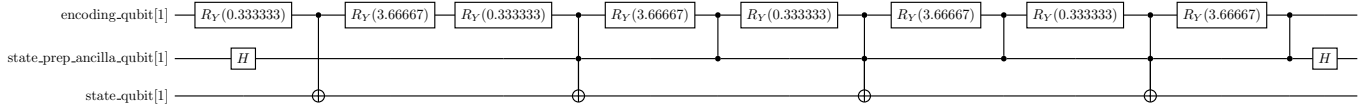


FIG. 5. State preparation circuit for the Linear Combination of Unitaries method.

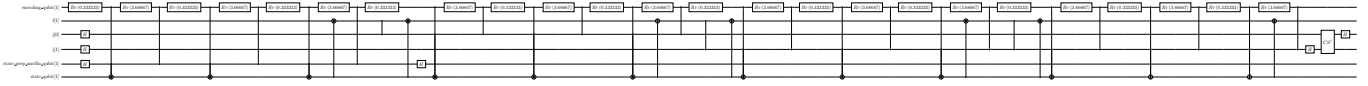


FIG. 6. Quantum Markov Chain Monte Carlo circuit using the Linear Combination of Unitaries method.

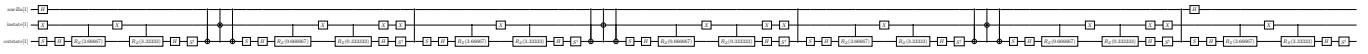


FIG. 7. Szegedy's method state preparation circuit. Size of 166 gates, including 92 PhasedX, 71 ZZPhase, and 3 measurements.

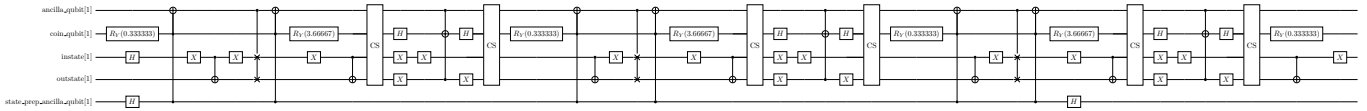


FIG. 8. Controlled-SWAP state preparation circuit. Size of 222 gates, including 126 PhasedX gates, 91 ZZPhase gates, and 5 measurements.

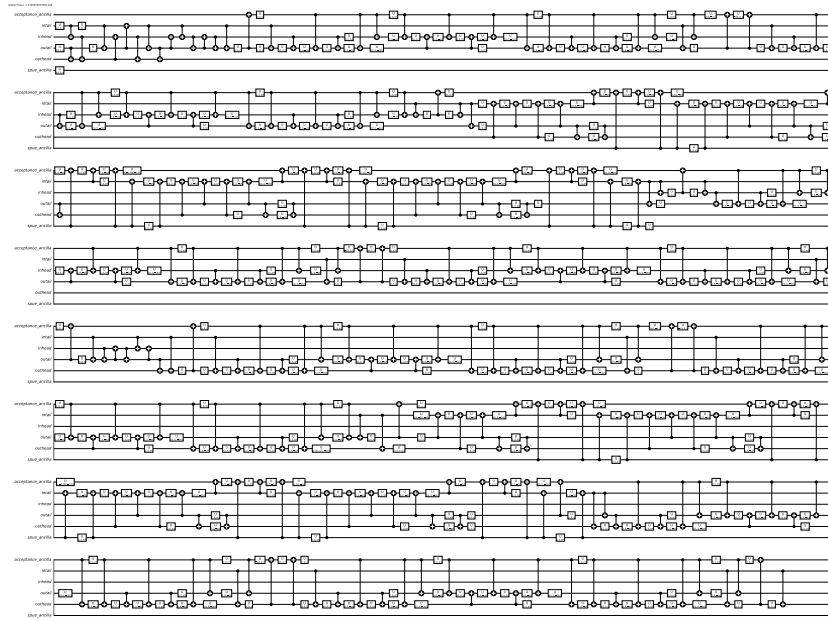


FIG. 9. Quantum circuit for the qubitized walk operator W of the dual Metropolis Hastings process [1].

Appendix B: Data

H2-1			Helios		
Outcome	Counts	Probability (%)	Outcome	Counts	Probability (%)
000	2586	25.86	010	2600	26.00
110	2462	24.62	110	2543	25.43
100	2447	24.47	100	2459	24.59
010	2376	23.76	000	2321	23.21
001	42	0.42	001	29	0.29
111	33	0.33	101	19	0.19
011	30	0.30	111	16	0.16
101	24	0.24	011	13	0.13

TABLE VI. State preparation using the linear combination of unitaries method on H2-1 (left) and Helios (right). The leftmost bit corresponds denotes the state in \mathbb{S} . The middle bit is 0 if the state preparation succeeded, 1 otherwise. The third qubit is the LCU ancilla.

H2-1			Helios		
Outcome	Counts	Probability (%)	Outcome	Counts	Probability (%)
111110	140	14.00	011000	134	13.40
101110	137	13.70	111110	122	12.20
011100	134	13.40	101110	121	12.10
001000	119	11.90	001100	118	11.80
111010	101	10.10	001000	115	11.50
101010	94	9.40	111010	111	11.10
001100	93	9.30	101010	99	9.90
011000	92	9.20	011100	99	9.90
010101	10	1.00	000101	7	0.70
000101	9	0.90	110111	6	0.60
110011	6	0.60	010001	6	0.60
000100	5	0.50	110010	4	0.40
100011	5	0.50	110011	4	0.40
110111	5	0.50	110110	4	0.40
010000	4	0.40	000100	4	0.40
010100	4	0.40	010000	4	0.40
101111	4	0.40	010100	4	0.40
110110	4	0.40	100110	3	0.30
000000	3	0.30	111100	3	0.30
000001	3	0.30	100010	3	0.30
001010	3	0.30	001001	3	0.30
001110	3	0.30	011101	2	0.20
110010	3	0.30	001110	2	0.20
010001	2	0.20	000110	2	0.20
011001	2	0.20	101011	2	0.20
100111	2	0.20	000001	2	0.20
101011	2	0.20	100011	2	0.20
111011	2	0.20	011001	1	0.10
111111	2	0.20	000000	1	0.10
001101	1	0.10	010101	1	0.10
011010	1	0.10	010010	1	0.10
100110	1	0.10	011010	1	0.10
101000	1	0.10	111111	1	0.10
101001	1	0.10	111011	1	0.10
110100	1	0.10	101111	1	0.10
111100	1	0.10	011110	1	0.10
			001101	1	0.10
			111000	1	0.10
			110100	1	0.10
			101100	1	0.10
			101000	1	0.10

TABLE VII. Phase estimation measurements on H2-1 (left) and Helios (right). Bit order from left to right: \mathbb{S} , state preparation ancilla, j_1 , j_0 , f , encoding qubit.

H2-1			Helios		
Outcome	Count	Probability (%)	Outcome	Count	Probability (%)
111	2007	20.07	000	2054	20.54
110	1779	17.79	111	1813	18.13
001	1766	17.66	110	1743	17.43
000	1711	17.11	001	1737	17.37
100	817	8.17	011	808	8.08
101	694	6.94	010	662	6.62
010	625	6.25	101	640	6.40
011	601	6.01	100	543	5.43

TABLE VIII. State preparation with Szegedy's method on H2-1 (left) and Helios (right). Bit order: out qubit - in qubit - state preparation ancilla.

H2-1			Helios		
Outcome	Count	Probability (%)	Outcome	Count	Probability (%)
01000	3457	34.57	00100	3527	35.27
00100	3238	32.38	01000	3286	32.86
01010	1297	12.97	00110	1330	13.30
00110	1282	12.82	01010	1262	12.62
01100	76	0.76	01100	79	0.79
10100	70	0.70	00000	58	0.58
00000	54	0.54	10100	49	0.49
11000	50	0.50	11000	48	0.48
00111	49	0.49	00101	46	0.46
00101	48	0.48	01001	43	0.43
10110	46	0.46	01011	33	0.33
01001	45	0.45	10110	33	0.33
01011	43	0.43	11001	26	0.26
11010	41	0.41	01110	25	0.25
10101	37	0.37	11010	24	0.24
00010	33	0.33	00010	23	0.23
01110	31	0.31	10101	16	0.16
11001	21	0.21	00111	15	0.15
10111	20	0.20	11110	14	0.14
00001	14	0.14	10111	11	0.11
11011	13	0.13	11011	10	0.10
11110	9	0.09	00001	9	0.09
00011	5	0.05	01101	8	0.08
01101	5	0.05	00011	5	0.05
10011	5	0.05	10001	5	0.05
11101	4	0.04	11100	4	0.04
01111	3	0.03	10011	3	0.03
10001	2	0.02	11101	2	0.02
10000	1	0.01	01111	2	0.02
10010	1	0.01	11111	2	0.02
			10010	1	0.01
			10000	1	0.01

TABLE IX. State preparation with the controlled-SWAP method on H2-1 (left) and Helios (right). Bit order: state preparation ancilla - in state - out state - coin qubit - S^c ancilla.

H2-1			H2-2			Helios		
Outcome	Count	Prob. (%)	Outcome	Count	Prob. (%)	Outcome	Count	Prob. (%)
110010	1290	12.90	101100	1311	13.11	110010	1262	12.62
110100	1285	12.85	001010	1259	12.59	101010	1254	12.54
001100	1267	12.67	001100	1258	12.58	010010	1251	12.51
101010	1266	12.66	010010	1243	12.43	001010	1229	12.29
101100	1233	12.33	101010	1230	12.30	110100	1208	12.08
001010	1203	12.03	110010	1222	12.22	001100	1197	11.97
010100	1193	11.93	010100	1216	12.16	101100	1196	11.96
010010	1171	11.71	110100	1204	12.04	010100	1187	11.87
010000	9	0.09	100100	8	0.08	110000	52	0.52
110000	9	0.09	100010	6	0.06	001000	50	0.50
111010	8	0.08	000010	5	0.05	010000	48	0.48
011100	7	0.07	000100	5	0.05	101000	45	0.45
111100	7	0.07	011100	4	0.04	111100	4	0.04
000010	6	0.06	101000	3	0.03	101110	3	0.03
011010	5	0.05	011010	3	0.03	011100	3	0.03
100100	5	0.05	111100	3	0.03	001101	2	0.02
000100	4	0.04	010110	2	0.02	100100	1	0.01
100010	4	0.04	110000	2	0.02	011010	1	0.01
101000	4	0.04	010000	2	0.02	000010	1	0.01
010101	3	0.03	110110	2	0.02	001011	1	0.01
101110	3	0.03	111010	2	0.02	000100	1	0.01
110110	3	0.03	001000	2	0.02	001110	1	0.01
001000	2	0.02	001011	2	0.02	101011	1	0.01
001110	2	0.02	110101	2	0.02	111010	1	0.01
010110	2	0.02	010011	1	0.01	110110	1	0.01
101101	2	0.02	110011	1	0.01			
110011	2	0.02	101011	1	0.01			
001011	1	0.01	101110	1	0.01			
001101	1	0.01						
010011	1	0.01						
101011	1	0.01						
110101	1	0.01						

TABLE X. Measurements of $V|0\rangle$ on Quantinuum devices H2-1, H2-2, and Helios. The bits denote, from left to right: the SPUE ancilla, outhead, outtail, intail, inhead, and coin ancilla.

H2-1			H2-2			Helios		
Outcome	Count	Prob. (%)	Outcome	Count	Prob. (%)	Outcome	Count	Prob. (%)
001010	1040	10.40	110010	1114	11.14	110010	1155	11.55
101100	1028	10.28	101100	1103	11.03	101100	1082	10.82
001100	1006	10.06	001010	1018	10.18	001100	1076	10.76
110100	1003	10.03	001100	1013	10.13	010010	1064	10.64
010100	960	9.60	010100	975	9.75	101010	1026	10.26
010010	938	9.38	010010	973	9.73	001010	1007	10.07
110010	934	9.34	101010	901	9.01	010100	956	9.56
101010	915	9.15	110100	899	8.99	110100	945	9.45
110011	79	0.79	110000	89	0.89	110011	79	0.79
101110	76	0.76	101110	73	0.73	110110	77	0.77
001000	75	0.75	000101	70	0.70	101110	60	0.60
010011	74	0.74	010000	69	0.69	101111	58	0.58
001101	71	0.71	101101	62	0.62	101101	54	0.54
101011	67	0.67	010011	62	0.62	111101	49	0.49
001001	64	0.64	111011	61	0.61	001110	48	0.48
110000	64	0.64	100101	63	0.63	101000	46	0.46
101001	63	0.63	001000	57	0.57	001101	44	0.44
101101	63	0.63	101000	56	0.56	110000	43	0.43
010111	59	0.59	010110	55	0.55	110001	42	0.42
110111	58	0.58	110011	55	0.55	011010	41	0.41

TABLE XI. Measurements of $\mathcal{WV}|0\rangle$ on Quantinuum devices H2-1, H2-2, and Helios. The bits denote, from left to right: the SPUE ancilla, outhead, outtail, intail, inhead, and coin ancilla.